Indirect L to T point optical transition in bismuth nanowires

Citation: Levin, A. J., M. R. Black, and M. S. Dresselhaus. "Indirect L to T point optical transition in bismuth nanowires." Physical Review B 79.16 (2009): 165117. © 2009 The American Physical Society.

As Published: http://dx.doi.org/10.1103/PhysRevB.79.165117

Publisher: American Physical Society

Persistent URL: http://hdl.handle.net/1721.1/51746

Version: Final published version: final published article, as it appeared in a journal, conference proceedings, or other formally published context

Indirect L to T point optical transition in bismuth nanowires

A. J. Levin,[1,*] M. R. Black,[2] and M. S. Dresselhaus[1,3]
[1]*Department of Physics, Massachusetts Institute of Technology, Cambridge, Massachusetts 02139-4307, USA*
[2]*Bandgap Engineering Inc., Waltham, Massachusetts 02451, USA*
[3]*Department of Electrical Engineering and Computer Science, Massachusetts Institute of Technology, Cambridge, Massachusetts 02139-4307, USA*

(Received 12 November 2008; revised manuscript received 11 February 2009; published 28 April 2009)

An indirect electronic transition from the L point valence band to the T point valence band has been previously observed in Bi nanowires oriented along the $[01\bar{1}2]$ crystalline direction (used by Black *et al.* and by Reppert *et al.*) but not in $[11\bar{2}0]$-oriented nanowires (used by Cornelius *et al.*) or in bulk bismuth. Here we measure the Bi nanowire samples from each of these prior experimental studies on the same Fourier transform infrared apparatus, confirming that the differences are indeed physical and are not associated with the experimental setup. We develop an analytical model for the threshold energy of the indirect L to T point valence-band transition that takes as parameters the nanowire diameter and crystalline orientation. Our model shows good agreement with experimental results, and demonstrates that the nonparabolic nature of the L point bands is essential for calculating the energy of this transition. Finally, we propose a mechanism based on symmetry lowering to explain why this indirect transition is observed for $[01\bar{1}2]$-oriented but not for $[11\bar{2}0]$-oriented nanowires.

DOI: 10.1103/PhysRevB.79.165117 PACS number(s): 73.21.Hb, 78.20.Bh, 78.67.Lt, 81.07.Vb

I. INTRODUCTION

Due to the unique electronic properties of bismuth, Bi nanowires provide an attractive low-dimensional system for studying quantum confinement effects, and these nanowires have therefore generated much interest for both optical and thermoelectric applications. Two especially interesting features of Bi nanowires are the nonparabolic nature of the electronic energy bands near the Fermi level and the large anisotropy of the carrier pockets. As a result of these features, the electronic properties of Bi nanowires depend strongly on both crystalline orientation and nanowire diameter.

Black *et al.*[1] investigated a sharp and intense absorption peak in Bi nanowires oriented along the $[01\bar{1}2]$ crystalline direction, a feature not observed in bulk bismuth. They found the energy of this absorption peak to be 965 and 1090 cm^{-1} in their samples with average wire diameters of 200 and $\sim$45 nm, respectively (see Fig. 1). Black *et al.*[1] explained this energy feature as an indirect transition from electronic states in the L point valence band to unoccupied states above the Fermi energy in the T point valence band. In this case, the L and T point subbands both decrease in energy with decreasing wire diameter but the L point subbands decrease in energy faster than the T point subbands due to the lower effective mass at the L points. Hence, the energy peak of this indirect interband transition increases with decreasing diameter but not as rapidly as would be expected of a direct interband or intersubband transition. Although this indirect transition (which we shall hence call the L-T transition) may occur in bulk Bi, it is not easily observable because the optical absorption in bulk Bi is dominated by the direct L point transition and by free-carrier absorption processes. In their paper, Black *et al.*[1] presented a numerical simulation of the L-T transition, which demonstrated good agreement with experimental results.

A further blueshift of this peak was reported for $\sim$10 nm Bi nanorods by Reppert *et al.*[2] (see Fig. 2). Here the infrared band is clearly resolved into a main absorption peak centered around 1393 cm^{-1}, as well a second smaller peak at 1460 cm^{-1}. This second peak is identified with an indirect process in which the incident photon energy is used to create a phonon spanning the L and T points in the Brillouin zone, as well as a photon of energy of 1393 cm^{-1} to excite an electron from the L point valence band to the T point valence band. An additional third absorption peak is seen as a weak shoulder at 1355 cm^{-1}, and is identified with the absorption of a phonon spanning the L and T points, and the excitation of an electron from the L to T points in the Brillouin zone. This feature is expected to be weak due to the low probability of having a 70 cm^{-1} phonon thermally excited at 300 K.[3]

In Sec. II, we present a simple analytical model for the threshold energy of the L-T transition that takes as parameters the wire diameter and crystalline orientation. Our model agrees very well with the above experimental results of Black *et al.*[1] and Reppert *et al.*,[2] and demonstrates that the nonparabolic nature of the L point bands is essential for calculating the energy of the L-T transition.

In another experiment, Cornelius *et al.*[4] did not observe the absorption peak near 1000 cm^{-1} in their study of $[11\bar{2}0]$-oriented Bi nanowires. Instead, their infrared spectra of nanowires with diameters ranging from 30 to 200 nm display an absorption peak that shifts from 2000 to 4000 cm^{-1}, and is consistent with a direct L-L point electronic transition.[3] However, since the samples of Cornelius *et al.*,[4] Reppert *et al.*,[2] and Black *et al.*[1] were all measured on different FTIR setups, it is possible that these differing results could stem from differences in experimental setup. In Sec. III, we measure samples from each of these three groups on the same FTIR apparatus, confirming that these differences are indeed physical and are not associated with the experimental setup.

We then propose a mechanism in Sec. IV to explain why this L-T transition peak is observed in $[01\bar{1}2]$-oriented but

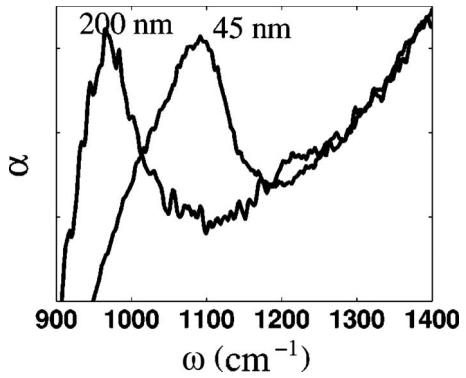

FIG. 1. Room temperature absorption peaks of Black *et al.*'s (Ref. 1) Bi nanowire samples (oriented in the $[01\bar{1}2]$ crystalline direction). The absorption α (arbitrary units) has been plotted as a function of wave number, ω.

not in $[11\bar{2}0]$-oriented nanowires. In our mechanism, the symmetry lowering caused by the finite lattice in the direction perpendicular to the nanowire axis allows for coupling between states which in the bulk are associated with different points in the Brillouin zone. In particular, under certain conditions one of the three L points can couple to the T point through the nanowire boundary, and the L-T transition would therefore no longer require a phonon for momentum conservation. In order for this to occur, one part of the nanowire boundary must be oriented in the proper direction to couple one of the L points to the T point, and we show that this is the case for $[01\bar{1}2]$-oriented but not $[11\bar{2}0]$-oriented Bi nanowires.

II. THEORETICAL MODELING

A. L-T transition

In bulk Bi, electron carrier pockets are three ellipsoids centered at the L points, and the hole carrier pocket is an ellipsoid of revolution centered at the T point whose axes coincide with the high-symmetry crystal axes (Fig. 3). Since the Bi crystal has trigonal symmetry, there are three equivalent L points and one T point. The constant energy hole ellipsoid at the T point may be characterized by the effective-mass tensor at the valence-band edge, written in Cartesian coordinates (where the x, y, and z coordinates correspond to the binary, bisectrix, and trigonal axes, respectively):

$$M_h = \begin{bmatrix} m_{h1}^* & 0 & 0 \\ 0 & m_{h2}^* & 0 \\ 0 & 0 & m_{h3}^* \end{bmatrix}. \tag{1}$$

We have $m_{h1}^* = m_{h2}^*$ due to symmetry, and $m_{h3}^* \gg m_{h1}^*$, indicating a large anisotropy in the T point hole Fermi surface. At 0 K, the effective-mass components are $m_{h1}^* = m_{h2}^* = 0.059$ and $m_{h3}^* = 0.634$ (in units of the free-electron mass m_0).[5] The T point effective-mass values are not expected to have a strong temperature dependence.[6]

The valence band at the T point is well approximated by a parabolic dispersion relation:

$$E_T(\vec{k}) = E_{T,0} - \frac{\hbar^2}{2m_0}\vec{k}\cdot M_h^{-1}\cdot\vec{k}, \tag{2}$$

where $E_{T,0}$ is the energy at the T point valence-band edge, m_0 is the free-electron mass, and M_h^{-1} is the inverse of the T point hole effective-mass tensor in Eq. (1).

The dispersion relations for the L point carriers are more complicated. To begin with, the principal axes of the L point ellipsoids are not aligned with the trigonal and bisectrix axes, and the effective-mass tensor is therefore not diagonal in Cartesian coordinates. The L point electron pocket shown in Fig. 3 is characterized by its effective-mass tensor

$$M_e = \begin{bmatrix} m_{e1}^* & 0 & 0 \\ 0 & m_{e2}^* & m_{e4}^* \\ 0 & m_{e4}^* & m_{e3}^* \end{bmatrix}. \tag{3}$$

At 0 K, the effective-mass components are $m_{e1}^* = 0.00113$, $m_{e2}^* = 0.26$, $m_{e3}^* = 0.00443$, and $m_{e4}^* = 0.0195$.[7] The L point band structure, in contrast to that of the T point, has a strong temperature dependence for temperatures above 80 K due to coupling between the nonparabolic L point valence and conduction bands.[6,8] As a result, the L point effective-mass components have been found to vary with temperature approximately according to the empirical relation[6]

$$m^*(T) = \frac{m^*(0)}{1 - 2.94\times10^{-3}T + 5.56\times10^{-7}T^2}, \tag{4}$$

obtained from magnetoreflection studies.

For $T = 300$ K, Eq. (4) yields $m^*(300) = 5.951\times m^*(0)$ so the L point effective-mass components at room temperature are taken to be $m_{e1}^* = 0.00672$, $m_{e2}^* = 1.547$, $m_{e3}^* = 0.02636$, and $m_{e4}^* = 0.116$. The other two L point pockets are obtained by 120° rotations of M_e about the trigonal (z) axis.

As noted above, the L point valence and conduction bands are very strongly coupled due to the small band gap between them [$E_{gL} = 36$ meV at 300 K (Ref. 6)], and a parabolic dispersion relation is therefore not appropriate. Instead, the L point band structure is best described by the two-band Lax model, which makes use of $\vec{k}\cdot\vec{p}$ perturbation theory.[9]

Taking the L point conduction-band edge as the zero value of the energy, the Lax model gives the following nonparabolic dispersion relations:

$$E_L(\vec{k}) = -\frac{E_{gL}}{2}\left(1 \pm \sqrt{1 + \frac{2\hbar^2}{m_0 E_{gL}}\vec{k}\cdot M_e^{-1}\cdot\vec{k}}\right), \tag{5}$$

where the + and − signs describe the dispersion relations of the L point valence and conduction bands, respectively, which are mirror images of each other due to their strong coupling in bulk bismuth. We use this basic model to handle the corresponding dispersion relations in the nanowires, which maintain the same crystal structure as bulk bismuth, with the same lattice constants, down to at least 7 nm in diameter.[10]

The electronic features of Bi nanowires differ from those of bulk bismuth due to quantum confinement, which causes the valence and conduction bands at the L and T points to

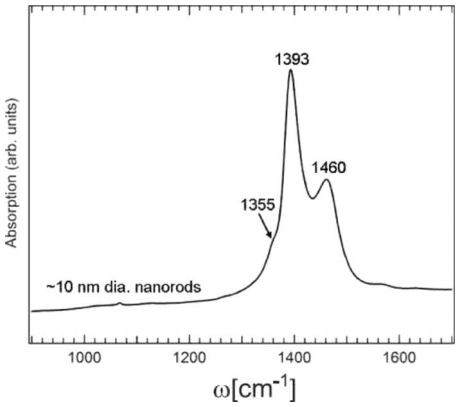

FIG. 2. IR absorption spectrum taken by Reppert *et al.* (Ref. 2) of the as-prepared ~10 nm Bi nanorods.

split into subbands. As the nanowire diameter decreases, the lowest L point conduction subband increases in energy as the highest valence subband correspondingly decreases in energy. This effectively increases the L point band gap, $E_{g\mathrm{L}}(d)$, which becomes a function of nanowire diameter d. At the same time, the highest T point valence subband decreases in energy, lowering the band overlap. For nanowires of diameter ~20 nm (depending on wire orientation), the band overlap becomes zero at room temperature, and the semimetal-semiconductor transition is reached.[11]

In a nanowire, the subbands of parabolic $E(\vec{k})$ bands (such as the T point valence band) split apart in energy proportionally to $\hbar^2/(m_p^* d^2)$, where m_p^* is the in-plane effective mass of the nanowire (for a given carrier pocket) and depends on crystalline orientation. However, as we shall show in the next section, the subbands of nonparabolic bands such as those at the L point in Bi do *not* split apart in energy proportionally to $\hbar^2/(m_p^* d^2)$, and this first-order approximation becomes increasingly inappropriate with decreasing nanowire diameter.

Here, we derive a formula for the threshold energy of the L-T transition. For simplicity, we will find the energy from the band edge of the highest L point valence subband to the band edge of the highest T point valence subband. This is a reasonably accurate approximation for the L-T transition energy,[1] but a complete treatment of energies associated with different subbands would require joint-density-of-states calculations, as well as a more in-depth study of the coupling and selection rules at the L and T points of the Brillouin zone.

From the schematic view of the electronic band structure of bulk Bi near the Fermi energy in Fig. 3, it can be seen that the energy difference between the L and T point band edges in bulk Bi can be expressed as $E_{g\mathrm{L}}+E_0$. The situation remains the same in nanowires, except that the highest valence subbands at both the L and T points decrease in energy due to quantum confinement. We will call $\Delta E_{\mathrm{L}}(d)$ the energy difference between the band edges at the L point of the valence band in bulk Bi and at the highest L point valence subband of a nanowire of diameter d. The corresponding term at the T point will be $\Delta E_{\mathrm{T}}(d)$. Hence, for the case of nanowires we obtain the following formula for the threshold energy of the L-T transition:

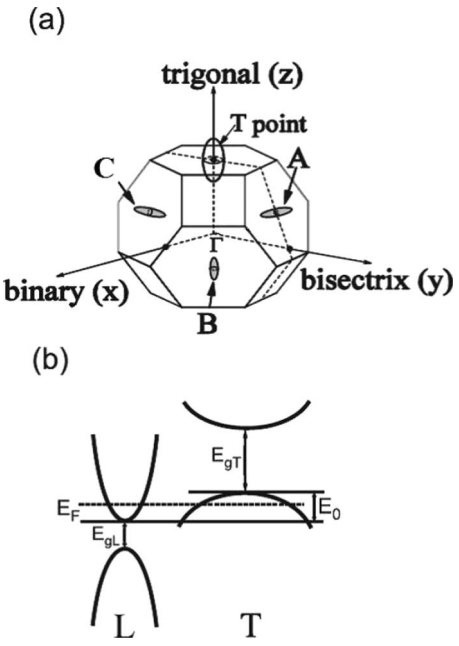

FIG. 3. (a) The Brillouin zone of bismuth, showing the T point hole pocket and the three L point electron pockets. (b) A schematic of the bismuth band structure near the Fermi level, indicating the direct band gap at the L point ($E_{g\mathrm{L}}$) and at the T point ($E_{g\mathrm{T}}$), as well as the band overlap E_0 from the T point valence-band edge to the L point conduction-band edge.

$$E_{\mathrm{L\text{-}T}}(d) = E_{g\mathrm{L}} + E_0 - \Delta E_{\mathrm{L}}(d) + \Delta E_{\mathrm{T}}(d). \tag{6}$$

In the following sections we will further analyze Eq. (6), and calculate the dependence of $E_{\mathrm{L\text{-}T}}(d)$ on crystalline orientation.

B. Square wire model

We are now ready to introduce an analytical model for calculating $E_{\mathrm{L\text{-}T}}(d)$. Since $E_{g\mathrm{L}}$ and E_0 are constants, we can focus on computing $\Delta E_{\mathrm{L}}(d)$ and $\Delta E_{\mathrm{T}}(d)$. In order to avoid numerical simulation and to keep our model analytical, we will treat the case of square nanowires instead of cylindrical ones. To ensure the accuracy of our results, we align the sides of the square wire with the directions of the two principal effective-mass components in the plane normal to the wire axis.

We perform calculations for square wires of side length d, treating the nanowire as an infinite potential well. The square wire model is easy to implement, and the infinite potential assumption is generally quite accurate since the nanowires we study are electrically isolated due to protective oxide coatings, dielectric mismatches with the outside environment, etc.

Since electron motion in nanowires is restricted in directions normal to the wire axis, quantum confinement causes the energies associated with the in-plane motion to be quantized. For a nanowire with a given crystalline orientation, let $m_{\mathrm{T},p}^*$ be the average in-plane effective mass at the T point, and $m_{\mathrm{L},p}^*$ be the average in-plane effective mass at the L point (we will calculate these values shortly). Let z' be the direc-

tion of the nanowire axis, and let x' and y' be two arbitrary directions in the plane of the nanowire cross section which are normal to each other. We will let the sides of the square wires be oriented along the x' and y' directions. The vector $\vec{k}$ in Eqs. (2) and (3) will have components $k_{x'}$, $k_{y'}$, and $k_{z'}$ in the orthogonal coordinate system $\{x', y', z'\}$. Due to quantum confinement in an infinite potential well, the values of $k_{x'}$ and $k_{y'}$ will be quantized:

$$k_{x'} = k_{y'} = \frac{n\pi}{d}. \tag{7}$$

For the highest valence subband, as we are considering, we have $n=1$. To find $\Delta E_{\mathrm{T}}(d)$, we use Eq. (2), noting that $k_{z'}=0$ at the band edge:

$$\begin{aligned}\Delta E_{\mathrm{T}}(d) &= E_{\mathrm{T}}(d) - E_{\mathrm{T},0} \\ &= -\frac{\hbar^2}{2m_0}\vec{k}\cdot M_h^{-1}\cdot\vec{k} \\ &= -\frac{\hbar^2}{2m^*_{\mathrm{T},p}m_0}(k_{x'}^2 + k_{y'}^2).\end{aligned} \tag{8}$$

Now, we can substitute Eq. (7) into Eq. (9):

$$\Delta E_{\mathrm{T}}(d) = -\frac{\hbar^2}{2m^*_{\mathrm{T},p}m_0}\left(2\frac{\pi^2}{d^2}\right) = -\frac{h^2}{4m^*_{\mathrm{T},p}m_0 d^2}. \tag{9}$$

Similarly, we use Eq. (5) to obtain $\Delta E_{\mathrm{L}}(d)$ for the nonparabolic L point valence band:

$$\begin{aligned}\Delta E_{\mathrm{L}}(d) &= \frac{E_{g\mathrm{L}}}{2}\left(1 - \sqrt{1 + \frac{2\hbar^2}{m_0 E_{g\mathrm{L}}}\vec{k}\cdot M_e^{-1}\cdot\vec{k}}\right) \\ &= \frac{E_{g\mathrm{L}}}{2}\left(1 - \sqrt{1 + \frac{1}{E_{g\mathrm{L}}}\frac{h^2}{m^*_{\mathrm{L},p}m_0 d^2}}\right).\end{aligned} \tag{10}$$

The expressions $\Delta E_{\mathrm{T}}(d)$ and $\Delta E_{\mathrm{L}}(d)$ in Eqs. (9) and (10) can be inserted into Eq. (6), along with the bulk values $E_{g\mathrm{L}}$ and E_0, to find the transition energy $E_{\mathrm{L\text{-}T}}(d)$. We will now use solid geometry to find the in-plane effective-mass values $m^*_{\mathrm{L},p}$ and $m^*_{\mathrm{T},p}$ given a nanowire axis direction, leaving d as the only variable in Eq. (6).

C. Calculating the in-plane effective mass

Recall that the L and T point carrier ellipsoids are characterized (in Cartesian coordinates) by their respective band-edge effective-mass tensors M_e and M_h given in Eqs. (1) and (3). Given a nanowire direction, we can use M_e and M_h to calculate the average in-plane masses $m^*_{\mathrm{L},p}$ and $m^*_{\mathrm{T},p}$, respectively. For the sake of generality, we will refer to the effective-mass tensor M, and the corresponding average in-plane effective mass m_p^*, for a given carrier pocket.

Following the reasoning in Ref. 11, for a carrier pocket with effective-mass tensor M, the in-plane effective mass m_p^* of the nanowire can be accurately given as

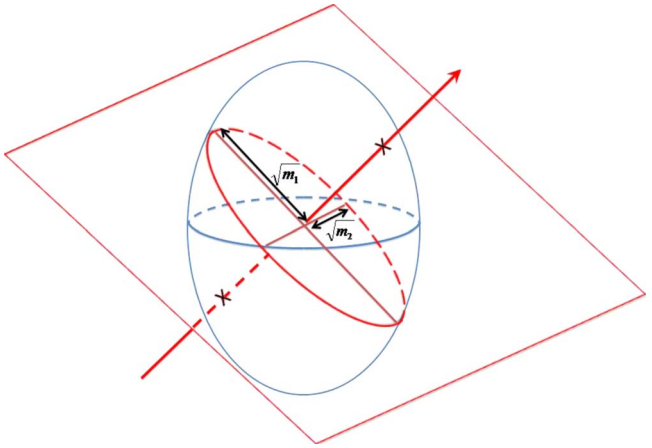

FIG. 4. (Color online) The intersection of an ellipsoid with a plane is a two-dimensional ellipse. Given the carrier ellipsoid described in Eq. (12), the half-axis lengths of the resulting ellipse are $\sqrt{m_1^*}$ and $\sqrt{m_2^*}$ as shown in the figure.

$$\frac{1}{m_p^*} \sim \frac{1}{2}\left(\frac{1}{m_1^*} + \frac{1}{m_2^*}\right), \tag{11}$$

where m_1^* and m_2^* are the two principal effective-mass components in the plane normal to the nanowire axis. A quick calculation shows that this designation is equivalent to setting the orientations x' and y' of the square wire sides along the directions of the two principal in-plane mass components m_1^* and m_2^*.

Given a nanowire whose axis may be represented by the vector $[a,b,c]$ in Cartesian coordinates, the intersection of the plane normal to the nanowire axis with the carrier ellipsoid will be an ellipse, as shown in Fig. 4. The lengths of the half axes of this ellipse will thus be exactly $\sqrt{m_1^*}$ and $\sqrt{m_2^*}$, where m_1^* and m_2^* are the two principal effective-mass components in the plane normal to the nanowire axis. Thus, by Eq. (11) we must find the lengths of the half axes of this ellipse in order to calculate m_p^*.

The calculation of m_p^* can be rephrased as a problem in solid geometry: given an ellipse formed by the intersection of an ellipsoid and a plane, which are defined, respectively, by the equations:

$$[x \quad y \quad z][M^{-1}]\begin{bmatrix} x \\ y \\ z \end{bmatrix} = 1, \tag{12}$$

$$ax + by + cz = 0, \tag{13}$$

where a, b, and c are the Cartesian components of a vector perpendicular to the plane (representing the nanowire axis), we find the lengths of the semimajor and semiminor axes of this ellipse.

We can solve this problem using the following procedure:

(1) Use Eq. (13) to find $z(x,y)$ (z in terms of x and y).

(2) Choose new coordinates $x'(x,y)$ and $y'(x,y)$ that satisfy the criterion $x^2+y^2+z(x,y)^2=x'^2+y'^2$. The equation $d^2=x'^2+y'^2$ defines a distance metric on the plane given by Eq.

TABLE I. Values of the confined effective-mass components m_1^*, m_2^*, and the resulting values of m_p^* for each carrier pocket (in units of m_0), calculated for nanowires oriented in the $[01\bar{1}2]$ direction.

Pocket	T	L(A)	L(B)	L(C)
m_1^*	0.059	0.011	0.009	0.007
m_2^*	0.143	0.138	0.036	0.031
m_p^*	0.0835	0.020	0.014	0.011

(13). Any point P on the plane can now be given by its coordinates (x',y') instead of (x,y,z), and the square distance of P from the origin can be written as $d^2=x'^2+y'^2$ instead of $d^2=x^2+y^2+z^2$.

(3) Find the inverse relations $x(x',y')$ and $y(x',y')$.

(4) Substitute $z(x,y)$ from step (1) into Eq. (12), which becomes an equation of x and y. Now, insert into this equation the relations $x(x',y')$ and $y(x',y')$ from step (3) to obtain an equation for the ellipse in $\{x',y'\}$ coordinates.

(5) The equation for this ellipse most likely will not be diagonal in the $\{x',y'\}$ basis. It will have the form $k_1x'^2+2k_2x'y'+k_3y'^2=1$, for some constants k_1, k_2, and k_3. This equation can be elegantly written in matrix form as

$$\begin{bmatrix} x' & y' \end{bmatrix} \begin{bmatrix} k_1 & k_2 \\ k_2 & k_3 \end{bmatrix} \begin{bmatrix} x' \\ y' \end{bmatrix} = 1. \tag{14}$$

(6) Find the eigenvalues λ_1 and λ_2 of this 2×2 matrix. The quantities $\sqrt{(1/\lambda_1)}$ and $\sqrt{(1/\lambda_2)}$ are the half-axis lengths of the desired ellipse. Recalling that the half axes have lengths $\sqrt{m_1^*}$ and $\sqrt{m_2^*}$, we obtain our desired result:

$$m_1^* = \frac{1}{\lambda_1}; \quad m_2^* = \frac{1}{\lambda_2}, \tag{15}$$

which we can insert into Eq. (11) to obtain m_p^*.

This method is particularly robust because we can simply insert the Cartesian coordinates $[a,b,c]$ of *any* desired nanowire axis direction into Eq. (13), and proceed to calculate the corresponding in-plane effective mass.

Table I lists the values of m_1^*, m_2^*, and the resulting m_p^* obtained by the above procedure for the T point and for each of the three L points for wires oriented in the $[01\bar{1}2]$ direction. We obtain the three L point in-plane effective masses by inserting M_e^{-1} into Eq. (12), and using the Cartesian family of $[01\bar{1}2]$ directions $\{[-0.774,0.223,0.593]$, $[0.193,-0.782,0.593]$, $[0.580,0.558,0.593]\}$ derived in Ref. 12 as the components $[a,b,c]$ in Eq. (13). To obtain the T point in-plane effective mass $m_{T,p}^*$, we insert M_h^{-1} into Eq. (12), and use the vector coordinates $[-0.774,0.223,0.593]$ in Eq. (13).[12]

D. Results

Having found the in-plane effective masses at the T point and at the three L points, we can now use them to obtain the full expression for $\Delta E_L(d)$, where we have inserted Eqs. (9) and (10) into Eq. (6):

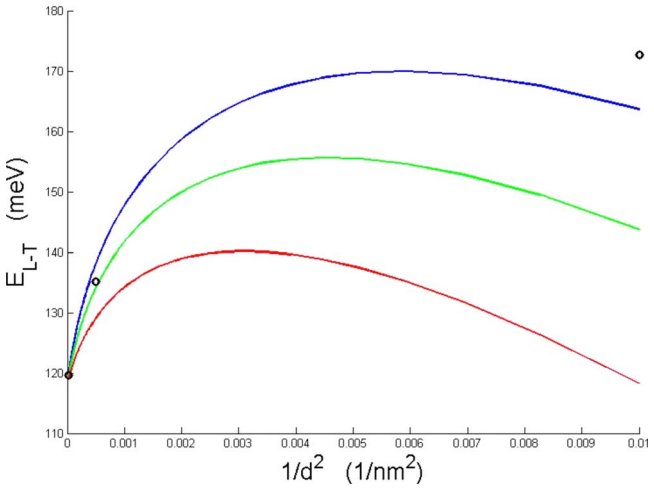

FIG. 5. (Color online) A plot of $E_{L\text{-}T}$ vs $1/d^2$ for the nonparabolic model, with d ranging from 300 to 10 nm. The blue curve (top) uses a value of $m_{L,p}^*=0.011$, the green curve (middle) uses $m_{L,p}^*=0.014$, and the red curve (bottom) uses $m_{L,p}^*=0.020$. The three experimental data points ($d=300$, 45, and 10 nm) and their respective energy peaks are plotted as black circles, and they fit best for $m_{L,p}^*=0.011$.

$$E_{L\text{-}T}(d) = E_{gL} + E_0 - \frac{E_{gL}}{2} \times \left(1 - \sqrt{1 + \frac{1}{E_{gL}} \frac{h^2}{m_{L,p}^* m_0 d^2}}\right) - \frac{h^2}{4 m_{T,p}^* m_0 d^2}. \tag{16}$$

One difficulty in implementing this model lies in the fact that the bulk bismuth band parameters are not accurately known at room temperature. The L point band gap and the L-T band overlap have been estimated to be $E_{gL}=36$ meV and $E_0=98$ meV, respectively, but since only one study measures these values, it is not clear how accurate these values are.[6] Since the value of E_{gL} is likely to be more accurate than the value of E_0, we will use the published value of $E_{gL}=36$ meV, and we will find E_0 using our model.

There are three experimental data points available that have been identified with the L-T transition, all for $[01\bar{1}2]$-oriented nanowires. As mentioned in Sec. I, Black *et al.*[1] measured peaks of 965 (119.6 meV) and 1090 cm^{-1} (135.1 meV) for nanowires with diameters of 200 and 45 nm, respectively, while the ~10 nm nanowires of Reppert *et al.*[2] had a large absorbance peak at 1393 cm^{-1} (172.7 meV).

To obtain a value of the band overlap E_0, we insert the values $E_{gL}=36$ meV, $m_{T,p}^*=0.0835$, and $m_{L,p}^*=0.014$ (the middle value of $m_{L,p}^*$ in Table I) into Eq. (16), for $d=200$ nm. This gives us a value of $E_0=82.5$ meV, which we shall now use in our calculations.

Note that the cross-sectional area of a cylindrical wire of diameter d is smaller by a factor of $\pi/4$ than the cross-sectional area of a square wire with side length d. Therefore, we have multiplied d^2 by $\pi/4$ in Eq. (16) in order to generate the plot in Fig. 5.

Let us now examine the parameters of our model in more detail. In Fig. 5, we have plotted $E_{L\text{-}T}$ vs $1/d^2$ for each of the

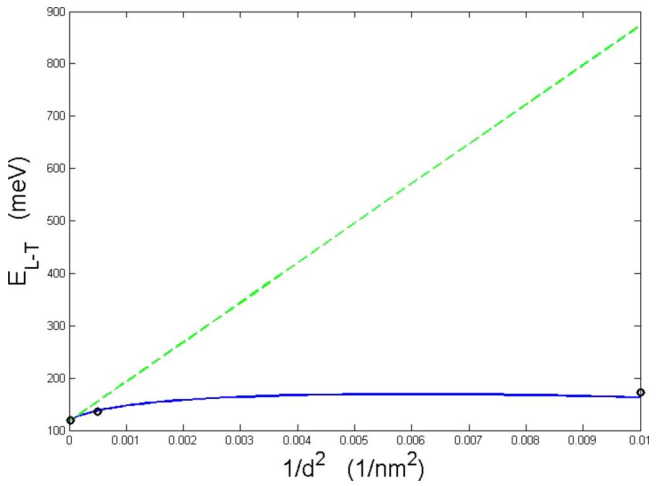

FIG. 6. (Color online) A plot of $E_{\text{L-T}}$ vs $1/d^2$ for the two models, with d ranging from 300 to 10 nm. The dashed curve shows the parabolic model of Eq. (18) while the solid curve shows the nonparabolic model of Eq. (16). The three experimental data points (d=300, 45, and 10 nm) and their respective energy peaks are plotted as black circles. The value of $m^*_{\text{L},p}$=0.011 was used throughout.

three in-plane L point masses in Table I. We have again included the three experimental data points for reference, and use the values E_0=82.5 meV and $E_{g\text{L}}$=36 meV. We see that our model agrees well with the experimental data. As we can see, the energy of the transition has a strong dependence on the value of $m^*_{\text{L},p}$.

Notice that the closest fit of our model with the experimental points is observed when we use the L(C)-point in-plane effective-mass value $m^*_{\text{L},p}$=0.011. This is consistent with the fact that the electron pocket with the smallest in-plane effective mass will have the largest transport effective mass m^*_l along the wire axis, and is therefore expected to have a large joint density of states and to contribute the most to optical absorption.

It is interesting to note that, below a certain nanowire diameter, our model predicts that the highest T point subband decreases in energy faster than the highest L point subband, thus *decreasing* the energy of the L-T transition. The value of this diameter depends on the in-plane effective masses $m^*_{\text{L},p}$ and $m^*_{\text{T},p}$.

In our model we have used the nonparabolic two-band Lax model for the dispersion relations at the L point in bismuth. We shall now demonstrate that the Lax model is much more appropriate than the parabolic model in describing the L point band structure, as the first-order parabolic approximation gives highly inaccurate results in our model. To see this, we expand $\Delta E_{\text{L}}(d)$ in Eq. (10) to first order about $k_{z'}$=0:

$$\Delta E_{\text{L}}(d) = -\frac{h^2}{4m^*_{\text{L}}m_0d^2}. \tag{17}$$

Inserting Eqs. (9) and (17) into Eq. (6), we obtain

$$E_{\text{L-T}}(d) = E_{g\text{L}} + E_0 + \frac{h^2}{4m^*_{\text{L},p}m_0d^2} - \frac{h^2}{4m^*_{\text{T},p}m_0d^2}. \tag{18}$$

In Fig. 6, we have plotted the energies of the L-T transition vs $1/d^2$ for the nonparabolic and the parabolic models, respectively, given by Eqs. (16) and (18), along with the three experimental data points mentioned above. We have used the values E_0=82.5 meV, $E_{g\text{L}}$=36 meV, $m^*_{\text{L},p}$=0.011, and $m^*_{\text{T},p}$=0.0835.

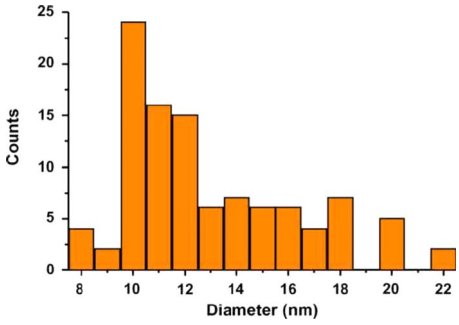

FIG. 7. (Color online) The diameter distribution of ~100 bismuth nanorods of Reppert *et al.* (Ref. 2).

It can be seen from Fig. 6 that the nonparabolic Lax model is far more appropriate than the parabolic model, which predicts a linear $E_{\text{L-T}}$ vs $1/d^2$ relation. Interestingly, the ~10 nm diameter nanorods of Reppert *et al.*[2] show the L-T transition even though their diameters are expected to fall below the semimetal-semiconductor (SM-SC) transition, which Lin *et al.*[11] predict to occur at 14.0 nm at 300 K for nanowires oriented in the $[01\bar{1}2]$ direction. Nanowires below the SM-SC transition diameter are semiconducting, as all the electron states in the T point valence band become filled, and so an electron from the L point valence band cannot be excited to a state near the T point band edge. Hence, the optical absorption from the L-T transition in undoped semiconducting nanowires is quenched. There are several possible explanations for the observation of the L-T transition in the ~10 nm wires:

(1) The SM-SC transition could actually occur at <10 nm in $[01\bar{1}2]$-oriented nanowires. This is unlikely because it would require a large correction to the known values of the effective masses at room temperature. Although these values are not well characterized, a large inaccuracy is unlikely.

(2) The samples of Reppert *et al.*[2] could be doped so as to lower the Fermi energy and open electron-accepting states at the T point. This doping could occur by unintentional impurities in the bismuth nanowires or by band bending at the surface of the nanowire. In their paper, Reppert *et al.*[2] mention the results of Huber *et al.*,[13] who propose that evanescent surface states may dominate the electronic properties of bismuth nanostructures, as a result of which the carrier density is increased and the nanowire is effectively doped (it still is a semiconductor but the Fermi energy crosses the band edge).

(3) A third possible explanation relies on the fact that the nanorods of Reppert *et al.*[2] are distributed about 10 nm but do not all have this diameter value. As shown in Fig. 7, about one in four of their nanowires actually have diameters >14 nm. It is possible that the peak associated with the L-T transition is only seen from these larger-diameter nanowires.

III. EXPERIMENTAL RESULTS

In order to verify that the differences between the infrared spectra of the $[01\bar{1}2]$-oriented nanowires (Black *et al.*[1] and Reppert *et al.*[2]) and of the $[11\bar{2}0]$-oriented nanowires (Cornelius *et al.*[4]) are physical and not experimental in nature, it was necessary to measure the spectra of samples from all three groups on the same experimental apparatus.

To perform our Fourier transform infrared (FTIR) measurements, we used a Nicolet Magna-IR 860 Fourier transform infrared spectrometer and a Nic-Plan IR Microscope with a 1.5 mm aperture. Data were taken in the range of 600–4000 cm^{-1} at 300 K, with a resolution of 2 cm^{-1}. The microscope stage on which the samples rested was not evacuated, and remained at room pressure. We note that, although the light incident on the sample is mostly normal to the plane of the sample, some of the light is incident at an angle. Nicolet reports that this angle can vary from 0°–40°. For each set of samples, we first describe the fabrication details, and then our experimental results.

The Bi nanowire samples of Black *et al.*[1] were prepared by template-assisted synthesis. First, anodic alumina templates were produced by anodizing pure Al in acid. Under carefully chosen conditions, a regular array of parallel and nearly hexagonal channels formed on the resulting oxide film. The channel diameter and length could be controlled by varying the anodization voltage and the acid etch time, respectively. The channels were then filled by high-pressure injection of liquid bismuth. Finally, the alumina template was etched away, leaving an array of free-standing bismuth nanowires. The resulting nanowires possess a high degree of crystallinity, and x-ray diffraction (XRD) measurements show a dominant crystal orientation along the $[01\bar{1}2]$ axis.

It must be noted that the etching of the alumina template leaves a significant bismuth oxide coating on the nanowires. For example, the "45 nm" diameter nanowires actually had a diameter of 60 nm inside the alumina template but Black *et al.*[1] measured a ~7 nm thick coating of bismuth oxide around the Bi crystal core in free-standing wires by scanning electron microscopy and hence estimated the diameter of the bismuth core to be ~45 nm.

Figure 8 shows a spectrum from one of Black *et al.*'s[1] nanowires in the reflection mode, where we have used a polished gold mirror as the background. We see that there is a large dip in reflectance in the vicinity of ~1000 cm^{-1}, which is not observed in bulk bismuth and corresponds to the L-T transition.

Reppert *et al.*[2] used an approach based on the pulse laser vaporization method to produce their samples. A Nd:yttrium aluminum garnet laser was used to ablate a rotating target of Bi powder (99.5%) and an Au catalyst. A continuous flow of argon and hydrogen gas caused the ablated material to flow downstream and collect on a water-cooled cold finger, where the Au particles served as a seed for the nanowire growth. After the reaction, the apparatus was cooled down to room temperature, and the ablated material was collected from the cold finger. The resulting deposit consisted predominantly of bismuth nanorods (short nanowires) with an average length of ~200 nm dispersed among spherical Bi nanoparticles and

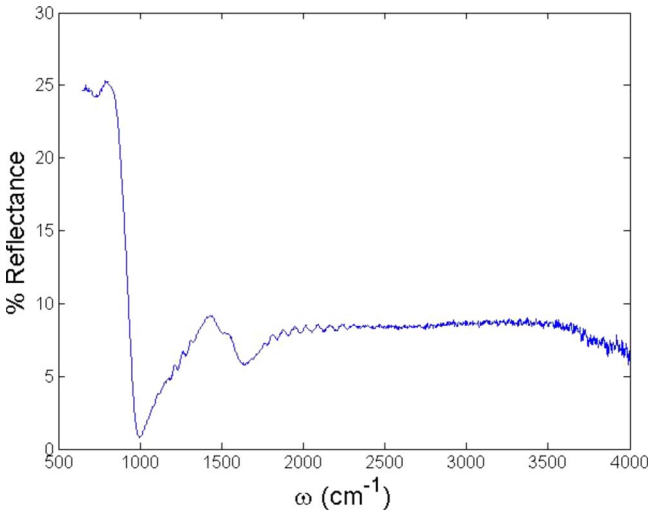

FIG. 8. (Color online) IR reflectance spectrum of one of Black *et al.*'s (Ref. 1) nanowire samples in alumina.

flat sheets of bismuth oxide. 3 mg of the nanorod deposit was then mixed with 50 mg of KBr powder, and the resulting mixture was pressed into a pellet 5 mm in diameter.

The nanorods contained a crystalline bismuth core encapsulated in a ~2 nm layer of Bi_2O_3. The predominant nanorod diameter was 10 nm, and XRD analysis showed a $[01\bar{1}2]$ nanorod growth direction. Moreover, the lattice spacing of the planes oriented along the length of the nanorods was found to be 0.328 nm, which is consistent with the $[01\bar{1}2]$ growth direction.

In Fig. 9 we have a transmission spectrum from the nanowire pellet of Reppert *et al.*[2] The peaks at 1393 and 1460 cm^{-1} are clearly visible, confirming that this feature is physical, and not related to differences in the experimental setup. The additional peak at ~850 cm^{-1} was observed by Reppert *et al.*[2] as well, and its origin is unclear.

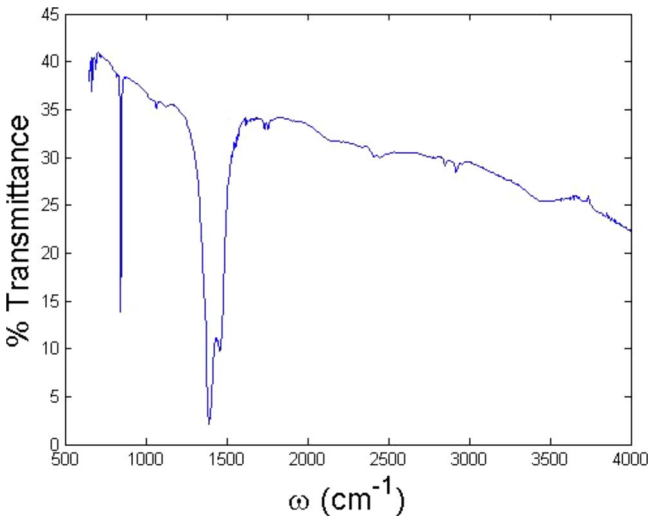

FIG. 9. (Color online) IR spectrum of the KBr pellet containing the nanorods of Reppert *et al.* (Ref. 2). Unlike the absorbance spectrum in Fig. 2, this spectrum is taken in the transmittance mode. To compare the two, note that $T(\omega)=1-A(\omega)$.

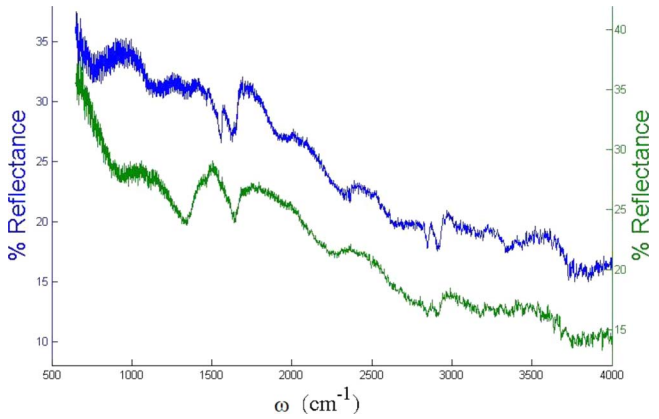

FIG. 10. (Color online) IR reflectance spectra of 100 and 40 nm Cornelius *et al.* (Ref. 4) samples. The reflectances of the 40 (top, blue) and the 100 nm samples (bottom, green) are shown on the left and right y axes, respectively.

Finally, the samples of Cornelius *et al.*[4] were created by irradiating polycarbonate foils with energetic heavy ions. The latent ion tracks were subsequently etched in NaOH, and the diameter of the resulting pores was controlled by the etching time. In the next step, a conductive electrode was deposited on one side of the polycarbonate membrane, and nanowires were grown electrochemically inside the pores. These nanowires were highly oriented along the $[11\bar{2}0]$ direction, as shown by transmission electron microscopy, XRD, and electron-diffraction measurements, and possessed a high degree of crystalline order. The membrane was then dissolved in dimethylformamide, and the wires were detached from the electrode by means of ultrasound. Several drops of the resulting solvent-nanowire suspension were put on a silicon wafer. The solvent completely evaporates at room temperature, leaving behind the nanowires.

For their FTIR measurements, Cornelius *et al.*[4] selected single nanowires by means of an aperture and took infrared transmission spectra, using as a reference nearby areas on the wafer without any nanowires. They did not notice any large absorption peaks in the 1000–1500 cm^{-1} range.

Figure 10 shows reflectance spectra we obtained from the 40 and 100 nm samples of Cornelius *et al.*,[4] mounted on silicon wafers. Since the resolution of our aperture was 1.5 mm, we could not select individual nanowires as they did, but instead measured spectra of an area containing the nanowires. We used a polished gold mirror as our background instead of a nanowire-free area of the wafer as they had done. However, the background spectra we measured from the gold mirror and from the silicon background looked very similar, so this difference cannot account for any qualitative differences between their spectra and ours.

It is difficult to extract quantitative features from these two spectra due to the large aperture spot size and the irregularity of the bismuth nanowire suspension droplet on the wafer surface. Nonetheless, we see that there are no large absorption features in the 1000–1500 cm^{-1} range, and we note an overall decrease in reflectance for frequencies larger than 2000 cm^{-1}. Thus, our results confirm that the L-T transition peaks visible in $[01\bar{1}2]$-oriented nanowires are absent in $[11\bar{2}0]$-oriented nanowires.

IV. COUPLING AT THE INTERFACE

The explanation we propose to account for the unexpectedly high intensity of the optical absorption from the indirect L-T transition in $[01\bar{1}2]$-oriented nanowires relates to the symmetry lowering, and thus to the breakdown of symmetry selection rules, of these bismuth nanowires. For electrons traveling in the direction perpendicular to the wire axis, the assumption of a periodic potential is no longer valid. Momentum is no longer a good quantum number, and states which in the bulk are orthogonal, now overlap partially. This allows for coupling between states which in the bulk are associated with different points in the Brillouin zone. Because of the coupling between these states in the nanostructure, the corresponding indirect electronic transitions would not require phonons for momentum conservation. The momentum change in the nanostructure is instead transferred to the boundary (the truncation of the lattice).

Classically speaking, this is similar to throwing a ball at an angle toward a wall. When the ball bounces off the wall, it goes in a different direction. If the wire boundary is in exactly the right direction, a ball thrown in the L point direction will bounce off in the T point direction. Therefore, near the surface the two directions can be coupled through the interface.

In order for the L and T points to couple, one part of the wall at the boundary of the wire needs to be oriented in the correct direction to couple one of the L points with the T point. Given a nanowire orientation, the question now becomes: how does one test if such a coupling exists?

In Cartesian (x,y,z) coordinates, the T point direction has coordinates [0,0,1], and the three L point directions L(A), L(B), and L(C) have coordinates [0,0.833,0.553], [−0.722, −0.417,0.553], and [0.722,−0.417,0.553], respectively[12] (in this paper, we have normalized the lengths of all relevant Brillouin-zone directions to one for convenience). Let the orientation of a nanowire under consideration be $[a,b,c]$ in Cartesian coordinates (for the wires we are interested in, $[01\bar{1}2]$ and $[11\bar{2}0]$ are $[-0.774,0.223,0.593]$ and $[-0.756,0.655,0]$ in Cartesian coordinates, respectively[12]).

If this nanowire has a surface that couples, say, the L(A) direction with the T direction [in other words, an electron traveling in the L(A) direction can bounce off the surface and end up traveling in the T direction], then the vector between these two directions, [L(A)−T], will be normal to this surface, assuming that the angle of incidence equals the angle of reflection. Now, if the nanowire *does*, in fact, have a surface with a normal vector [L(A)−T], then the nanowire axis $[a,b,c]$ will be orthogonal to this vector; in other words, the dot product of $[a,b,c]$ with the [L(A)−T] vector will be zero.

Thus, to check if a nanowire of orientation $[a,b,c]$ has a surface that couples one of the L points to the T point (or the negative T point), it is necessary to compute the six dot products $[\mathrm{L}(A)-\mathrm{T}]\cdot[a,b,c]$, $[\mathrm{L}(B)-\mathrm{T}]\cdot[a,b,c]$, $[\mathrm{L}(C)-\mathrm{T}]\cdot[a,b,c]$, $[\mathrm{L}(A)+\mathrm{T}]\cdot[a,b,c]$, $[\mathrm{L}(B)+\mathrm{T}]\cdot[a,b,c]$, and $[\mathrm{L}(C)+\mathrm{T}]\cdot[a,b,c]$. (By the inversion symmetry of the lattice, the negative T point is also a valid T point, and the negative L points are valid L points). If any of these six dot

TABLE II. Coupling between the L and T points for nanowires of different orientations. Each data point was calculated by first finding the vector between the two points indicated at the beginning of the row, then normalizing this vector, and finally taking the dot product of this normalized vector with the wire orientation vector. All calculations are done in Cartesian coordinates. Note that the entry in bold face is closest to zero.

Wire axis	$[01\bar{1}2]$	$[11\bar{2}0]$	$[10\bar{1}1]$	[0001]
L(A),T	**−0.084**	0.577	0.473	−0.473
L(B),T	0.212	0.288	−0.629	−0.473
L(C),T	−0.969	−0.865	−0.629	−0.473
L(A),−T	0.628	0.310	0.881	0.881
L(B),−T	0.787	0.155	0.290	0.881
L(C),−T	0.153	−0.464	0.290	0.881

products are zero (or sufficiently close to zero), then this nanowire has a wall in the correct direction to couple an L point to a T point and optical absorption should be observable for nanowires but not for bulk samples.

In Table II below, we have computed these dot products (after normalizing the six [L ± T] vectors) for nanowires of various orientations. Note that the Cartesian coordinates of $[10\bar{1}1]$ and [0001] wires are [0,0.833,0.553] and [0,0,1], respectively.[12]

One can see from Table II that the term closest to zero is found for the L(A) direction in $[01\bar{1}2]$-oriented nanowires, with a dot product value of −0.084. We expect states near the L point to couple with states near the T point, but since this number is not exactly zero, these states will not be right at the zone-boundary edge.

In order for an electronic transition to occur, a free state needs to be present at the T point. Since the Fermi energy is near the top of the valence band at the T point (42 meV in bulk bismuth[8] and less in nanowires due to quantum confinement), states farther away from the T point will be filled. A larger value in Table II indicates coupling farther away from the high-symmetry L and T points, and we expect weaker electronic transitions with dot products of increasing magnitude. This provides a plausible explanation for the fact that the L-T transition is expected in $[01\bar{1}2]$-oriented nanowires but not in nanowires of the other three common orientations (where the coupling may be too weak, or the T point electronic states filled), and also not in bulk bismuth.

Since the nanowires appear increasingly bulklike with increasing diameter, we expect this effect to be most pronounced for small diameter nanowires. However, it is interesting to consider the relevant length scales of the process. Since we are not dealing with a quantum confinement effect, the de Broglie wavelength is unlikely to be the length scale of importance. Furthermore, an electron traveling very far from the wire boundary should not experience the effects of the wire boundary, as it will scatter long before reaching it. The average distance that a carrier travels before undergoing a large-angle scattering event is the mean-free path, and so we expect that the relevant length scale is the mean-free path of bismuth.

V. CONCLUSIONS

We have calculated the energy difference between the L and T point valence-band edges as a function of nanowire diameter and crystalline orientation, and compared this result with the absorption features in previously published data, which are attributed to this electronic transition. Our simple infinite potential square-well model gives a good fit to the experimental data when nonparabolic dispersion relations are used at the L point, and leads us to conclude that the nonparabolicity of the L point energy bands is a key factor in interpreting optical effects in bismuth nanowires.

The in-plane effective-mass value, which we determined from the nanowire crystalline orientation and from the effective-mass tensor for each band, is set as a fitting parameter in our model. The best fit to the data occurs for $m_p^* = 0.011 m_0$, our smallest calculated in-plane effective mass. Since the smallest in-plane effective mass will have the largest effective mass in the direction of the wire axis and therefore in the transport direction, it is expected to have the largest joint density of states and to contribute the most to optical absorption.

By repeating measurements of three different groups on the same experimental setup, we have demonstrated that the previously observed differences between the infrared spectra of Bi nanowires oriented in the $[01\bar{1}2]$ and $[11\bar{2}0]$ directions are physical in nature, and were not caused by differences in experimental setup. We therefore conclude that the differences in the optical properties of the nanowires from the different groups are partly the result of the different crystalline orientations of their nanowires. We present a simple analytical model of the indirect L-T valence to valence band electronic transition and explain why this electronic transition could be the dominant optical property in nanowires of some crystalline orientations but is not observable in nanowires of other crystalline orientations. This model accounts for the differences between the optical data for the three different groups, and demonstrates the essential physics of this transition without the need for numerical simulation. Increasingly accurate measurements of the relevant bulk band parameters of bismuth are expected to increase the accuracy of our models. Future theoretical study of this L-T transition may elucidate the dependence of the energy of this transition on temperature and on doping.

ACKNOWLEDGMENTS

The authors thank A. M. Rao and J. Reppert for providing a bismuth nanorod sample, T. W. Cornelius and M. E. Toimil-Molares for providing bismuth nanowire samples, and both groups for valuable discussions. We are also grateful to Gene Dresselhaus for helpful discussions. Authors A.J.L. and M.S.D. acknowledge support from NSF Grant No. CTS-05-06830.

*Present address: Program in Molecular Biophysics, Johns Hopkins University, Baltimore, Maryland 21218, USA

[1] M. R. Black, P. L. Hagelstein, S. B. Cronin, Y. M. Lin, and M. S. Dresselhaus, Phys. Rev. B **68**, 235417 (2003).

[2] J. Reppert, R. Rao, M. Skove, J. He, M. Craps, T. Tritt, and A. M. Rao, Chem. Phys. Lett. **442**, 334 (2007).

[3] M. Black, J. Reppert, A. M. Rao, and M. S. Dresselhaus, *Optical Properties of Bismuth Nanostructures*, in Encyclopedia of Nanoscience and Nanotechnology, edited by H. S. Nalwa (to be published).

[4] T. W. Cornelius, M. E. Toimil-Molares, R. Neumann, G. Fahsold, R. Lovrincic, A. Pucci, and S. Karim, Appl. Phys. Lett. **88**, 103114 (2006).

[5] R. T. Isaacson and G. A. Williams, Phys. Rev. **185**, 682 (1969).

[6] M. P. Vecchi and M. S. Dresselhaus, Phys. Rev. B **10**, 771 (1974).

[7] G. E. Smith, G. A. Baraff, and J. M. Rowell, Phys. Rev. **135**, A1118 (1964).

[8] C. F. Gallo, B. S. Chandrasekhar, and P. H. Sutter, J. Appl. Phys. **34**, 144 (1963).

[9] B. Lax, J. G. Mavroides, H. J. Zeiger, and R. J. Keyes, Phys. Rev. Lett. **5**, 241 (1960).

[10] M. S. Dresselhaus, Y. M. Lin, O. Rabin, A. Jorio, A. G. Souza Filho, M. A. Pimenta, R. Saito, G. Samsonidze, and G. Dresselhaus, Mater. Sci. Eng., C **23**, 129 (2003).

[11] Y. M. Lin, X. Sun, and M. S. Dresselhaus, Phys. Rev. B **62**, 4610 (2000).

[12] A. J. Levin, Undergraduate thesis, MIT, 2008.

[13] T. E. Huber, A. Nikolaeva, D. Gitsu, L. Konopko, J. C. A. Foss, and M. J. Graf, Appl. Phys. Lett. **84**, 1326 (2004).